



**Dispersing nano- and micro-sized portlandite particulates
via electrosteric exclusion at short screening lengths**

Journal:	<i>Soft Matter</i>
Manuscript ID	SM-ART-01-2020-000045.R1
Article Type:	Paper
Date Submitted by the Author:	02-Mar-2020
Complete List of Authors:	<p>Timmons, Jason; University of California Los Angeles, Materials Science and Engineering Mehdipour, Iman; University of California Los Angeles Henry Samueli School of Engineering, Department of Civil and Environmental Engineering Gao , Shang ; University of California Los Angeles, Department of Chemical and Biomolecular Engineering Atahan, Hakan; Istanbul Technical University, Civil Engineering Neithalath, Narayanan; Arizona State University, School of Sustainable Engineering and the Built Environment Bauchy, M.; University of California Los Angeles, Garboczi, Edward; National Institute of Standards and Technology, Srivastava, Samanvaya; The University of Chicago, Institute for Molecular Engineering Sant, Gaurav; University of California, Los Angeles, Department of Civil and Environmental Engineering</p>

Revised for Submission to Soft Matter (March 2020)

1 **Dispersing nano- and micro-sized portlandite particulates via**
2 **electrosteric exclusion at short screening lengths**

3
4 *Jason Timmons (^{a,b,+}), Iman Mehdipour (^{b,+}), Shang Gao (^c), Hakan Atahan (^{b,d}), Narayanan Neithalath (^e),*
5 *Mathieu Bauchy (^{f,i}), Edward Garboczi (^g), Samanvaya Srivastava (^{c,i,**}), Gaurav Sant (^{a,b,h,i,**})*

^a Department of Materials Science and Engineering, University of California, Los Angeles, CA 90095, USA

^b Laboratory for the Chemistry of Construction Materials (LC²), Department of Civil and Environmental Engineering, University of California, Los Angeles, CA 90095, USA

^c Department of Chemical and Biomolecular Engineering, University of California, Los Angeles, CA 90095, USA

^d Department of Civil Engineering, Istanbul Technical University, Istanbul, Turkey

^e School of Sustainable Engineering and the Built Environment, Arizona State University, Tempe, AZ 86587, USA

^f Laboratory for the Physics of Amorphous and Inorganic Solids (PARISlab), Department of Civil and Environmental Engineering, University of California, Los Angeles, CA 90095, USA

^g Applied Chemicals and Materials Division, Material Measurement Laboratory, National Institute of Standards and Technology, Boulder, CO 80305, USA

^h California Nanosystems Institute (CNSI), University of California, Los Angeles, CA 90095, USA

ⁱ Institute for Carbon Management, University of California, Los Angeles, CA 90095, USA

⁺ Both authors contributed equally to this work.

****Corresponding authors:** S. Srivastava, Email: samsri@ucla.edu and G. Sant, Email: gsant@ucla.edu

Revised for Submission to Soft Matter (March 2020)

6

7 **Abstract**

8

9 In spite of their high surface charge (zeta potential $\zeta = + 34$ mV), aqueous suspensions of
10 portlandite (calcium hydroxide: $\text{Ca}(\text{OH})_2$) exhibit a strong tendency to aggregate, and thereby
11 present unstable suspensions. While a variety of commercial dispersants seek to modify the
12 suspension stability and rheology (e.g., yield stress, viscosity), it remains unclear how the
13 performance of electrostatically and/or electrosterically based additives is affected in aqueous
14 environments having either a high ionic strength and/or a pH close to the particle's isoelectric
15 point (IEP). We show that the high native ionic strength (pH ≈ 12.6 , IEP: pH ≈ 13) of saturated
16 portlandite suspensions strongly screens electrostatic forces (Debye length: $\kappa^{-1} = 1.2$ nm). As a
17 result, Coulombic repulsion alone is insufficient to mitigate particle aggregation and affect
18 rheology. However, a longer-range geometrical particle-particle exclusion that arises from
19 electrosteric hindrance caused by the introduction of comb polyelectrolyte dispersants is very
20 effective at altering the rheological properties and fractal structuring of suspensions. As a
21 result, comb-like dispersants that stretch into the solvent reduce the suspension's yield stress
22 by 5x at similar levels of adsorption as compared to linear dispersants, thus enhancing the
23 critical solid loading (i.e., at which jamming occurs) by 1.4x. Significantly, the behavior of
24 diverse dispersants is found to be inherently related to the thickness of the adsorbed polymer
25 layer on particle surfaces. These outcomes inform the design of dispersants for concentrated
26 suspensions that present strong charge screening behavior.

27

28 **Keywords:** *suspension rheology, aggregation, polymer adsorption, polyelectrolyte dispersant*

29

30 **1. Introduction**

31 The rheology of concentrated suspensions is important for many industrial processes. Colloidal
32 dispersions and gels exhibit a wide range of rheological properties such as aging, shear
33 thickening/thinning, and yielding. In particular, the yield stress and viscosity of suspensions
34 greatly affects the processing of materials for diverse applications including cement and
35 concrete pumping,^{1,2} gel casting of ceramics,^{3,4} drug delivery,^{5,6} as well as in emerging
36 technologies such as particulate flow batteries,^{7,8} and 3D-printing of slurries.^{9,10} However, on
37 account of their tendency to aggregate, the particles in a suspension may often organize into
38 flocs, and settle, resulting in undesirable behavior including a reduction of the maximum
39 (achievable) solid volume fraction (ϕ_{max}), and very high yield stress and viscosity that greatly
40 complicate suspension processing.^{11,12}

41

42 Generally, repulsive interactions between particles are introduced to enhance suspension
43 stability by: introducing charges on the particle surfaces (electrostatic repulsion),^{13,14} adsorbing
44 or grafting polymers onto particle surfaces to induce steric barriers,¹⁵⁻¹⁷ and combinations
45 thereof. However, even suspensions of strongly charged particles agglomerate readily,
46 especially in aqueous environments that present either a high ionic strength and/or a pH close
47 to the particle's isoelectric point (IEP). In such suspensions, strong screening of electrostatic
48 forces results in a sharp increase in yield stress with particle loading.¹⁸ As a result, the

Revised for Submission to Soft Matter (March 2020)

49 maximum achievable particle loadings (ϕ_{max}), i.e., prior to the onset of jamming (i.e., where
50 flow is arrested and the suspension exhibits solid-like behavior) remain modest.

51

52 Polyelectrolyte dispersants are often used to impart electrosteric barriers to particle
53 aggregation by forming an electrostatically adsorbed layer on particle surfaces that limits the
54 closest approach distance between adjacent particles.¹⁹ Thus, such dispersants act to reduce
55 the yield stress while simultaneously enhancing the maximum particle loadings of dense stable
56 suspensions. Steric barriers to particle aggregation are further accentuated by grafting non-
57 ionic side chains onto the adsorbing polyelectrolyte backbones to form ‘comb’
58 polyelectrolytes.^{20,21} The aqueous medium provides a good solvent for the side chains and they
59 extend into the solution, increasing the distance of the closest approach between particles.

60

61 While commercially available dispersants are often effective in altering suspension stability and
62 rheology, considerable challenges remain. For example, it remains difficult to design
63 dispersants for suspensions that self-regulate their pH and have high ionic strengths.²² This is
64 especially important when dispersants interact with the solution resulting in aggregation that
65 arises from ion bridging interactions and/or complexation between polymers and multivalent
66 counterions (e.g., Ca^{2+}).^{23–25} Portlandite (i.e., also known as slaked or hydrated lime or calcium
67 hydroxide: $\text{Ca}(\text{OH})_2$) is an example of such a solid, which in suspension, self-regulates its pH
68 (i.e., on account of its modest solubility; 20.3 mM at 25°C²⁶, $I_m = 60.9$ mM [molar ionic
69 strength], and rapid dissolution rate). Portlandite suspensions find use in applications including:
70 water treatment,^{27–29} dental fillings,^{30–32} food industry,^{33,34} and construction materials.^{35,36} On
71 account of the relatively high ionic strength resulting from its dissolution that can screen
72 electrostatic forces, portlandite often presents weakly-charged, unstable nanosized particulates
73 in suspension. This is problematic in applications where the suspension is required to have both
74 high particle volume fractions and amenable flow properties; their tendency to aggregate and
75 the low value of ϕ_{max} make processing difficult.¹¹ Therefore, this study seeks to elucidate: (a)
76 the mechanisms that affect the aggregation of portlandite suspensions, and (b) the interactions
77 between $\text{Ca}(\text{OH})_2$ suspensions and diverse dispersant chemistries that present varying
78 stabilization mechanisms (e.g., electrostatic and electrosteric), which produces varying
79 dispersant layer thicknesses. Focus is placed on identifying the characteristics of polymeric
80 dispersants that effectively improve the rheology of portlandite suspensions, and thereby offer
81 guidelines for the design of new dispersants for industrial applications.

82

83 **2. Materials and Methods**

84 **2.1. Materials and sample preparation**

85 Commercially available portlandite ($\text{Ca}(\text{OH})_2$; Standard Hydrated Lime, Mississippi Lime
86 Company)* was used. It featured a purity of 94 % \pm 2 % (by mass) with the remainder being
87 composed of CaCO_3 as determined by thermogravimetric analysis (TGA; STA 6000, Perkin

* Certain commercial equipment, software and/or materials are identified in this paper in order to adequately specify the experimental procedure. In no case does such identification imply recommendation or endorsement by the National Institute of Standards and Technology, nor does it imply that the equipment and/or materials used are necessarily the best available for the purpose.

Revised for Submission to Soft Matter (March 2020)

88 Elmer). The particle size distribution of the portlandite was measured using static light
89 scattering (SLS; LS13-320, Beckman Coulter), assuming a complex refractive index of $1.574 +$
90 $0.000i$.³⁷ The particulates were dispersed using ultrasonication in isopropanol (IPA), which was
91 used as the carrier fluid. The median particle diameter (d_{50}) of the particulates was estimated as
92 $3.8 \mu\text{m} \pm 0.2 \mu\text{m}$ (see Supplementary Information: Figure S1a). The density of the particulates
93 was measured as $2235 \text{ kg/m}^3 \pm 4 \text{ kg/m}^3$ using helium pycnometry (AccuPyc II 1340,
94 Micromeritics).

95
96 The morphology of the particles was examined using a field emission-scanning electron
97 microscope (FEI NanoSEM 230). All SEM micrographs were acquired in secondary electron
98 mode with a spot size of 4.0 nm, at an accelerating voltage of 10 kV, and a working distance of \approx
99 5.5 mm. The particles form aggregates whose size is similar to that measured by static light
100 scattering (see Supplementary Information: Figure S1b). Since light scattering is known to be
101 ineffective in determining the primary particle size of the aggregated portlandite
102 particulates,^{11,35} transmission electron microscopy (TEM; FEI T12 Quick CryoEM and CryoET)
103 was used to examine the primary particle size. A dilute suspension of portlandite particulates
104 robustly dispersed (with the application of ultrasonication) in IPA was deposited on to a TEM
105 grid; and the solvent was evaporated thereafter. Although large aggregates were still observed,
106 the primary particle size was established as being on the order of 20-to-200 nm (see
107 Supplementary Information: Figure S1c), as suggested previously.^{11,35,36} However, it was not
108 possible to meaningfully, on a statistical basis, resolve a sufficient number of non-agglomerated
109 particles to establish a particle size distribution from the TEM imaging of the primary
110 portlandite particles.

111
112 Three commercially available dispersants were used: (1) a polyacrylic acid-based dispersant
113 (PAA, Acumer 9000, Dow Chemical), (2) a lignosulfonate-based dispersant (LS, MasterPolyheed
114 997, BASF Corporation), and (3) a poly-carboxylate ether-based dispersant (PCE,
115 MasterGlenium 7500, BASF Corporation). The functional groups present in each polymer were
116 qualitatively determined (see Supplementary Information: Figure S2) using Fourier transform
117 infrared spectroscopy (FTIR; PerkinElmer Spectrum Two). In brief, LS contains sulfonic acid
118 groups,³⁸ PAA contains carbonyl groups, and PCE contains carbonyl groups associated with its
119 PAA backbone and ether groups corresponding to its polyethylene glycol (PEG) side chains
120 [N.B.: the ratio between the abundance of carbonyl-to-ether groups is 0.09:1; mass basis].³⁹
121 The solids content of each additive was determined as 49.03 mass %, 45.01 mass %, and 26.59
122 mass %, respectively. The molecular weight of the polymeric dispersants is provided in Table 1.
123 The dispersants were dosed at a level ranging between 0 mass % to 1.5 mass % of the total solid
124 content in the suspension, including the solids content of the polymer dispersant.

125
126 In order to prevent any complications caused by the dissolution of portlandite, a previously
127 saturated and filtered $\text{Ca}(\text{OH})_2$ solution was used as the suspending fluid. Saturated $\text{Ca}(\text{OH})_2$
128 solution was prepared by adding excess portlandite to deionized (DI) water, allowing for the
129 solids to settle, and then filtering the solution using a $0.20 \mu\text{m}$ syringe filter. To produce
130 suspensions, polymeric dispersants (when used) were added to the saturated $\text{Ca}(\text{OH})_2$ solution,
131 and then solid portlandite particulates were added to the solution. The mixtures were first

Revised for Submission to Soft Matter (March 2020)

132 mixed by hand, and then stirred for 120 s using a four-blade impeller-type high-shear mixer
133 (RW 20 Digital, IKA) at 500 rpm to produce well-dispersed and homogenous suspensions with
134 known particle volume fraction ϕ and dispersant dosage ρ (mass % of total solid, when used).

135

136 **2.2. Experimental methods**

137 *2.2.1. Characterization of polymers*

138 *Molecular Weight Characterization:* The molecular weight of the polymers was determined by
139 aqueous gel permeation chromatography (GPC; Waters Alliance 2695 Separation Module) with
140 a two-column setup (Shodex SB 804 HQ and Shodex SB 802.5 HQ). An evaporative light
141 scattering detector (ELSD; Alltech 3300) analyzed the polymer after elution in the GPC columns.
142 For quantitative analysis, external calibrations were carried out using narrow molecular weight
143 polyethylene glycol (PEG) standards ranging from 400 g/mol to 150,000 g/mol.

144 *Charge Density Characterization:* The charge density of the polymers was determined by
145 aqueous streaming current (Mütek PCD-05 Smart Particle Charge Detector) analyses. Each
146 polymer was diluted to the range of 100 ppm to 1,000 ppm and adjusted to pH = 12 by the
147 addition of sodium hydroxide (NaOH). These samples were then titrated with 0.001 N poly-
148 dimethyl-diallyl-ammonium chloride (polyDADMAC), until the streaming potential reached its
149 isoelectric point (charge = 0 mV). Based on the amount of polyDADMAC added to neutralize the
150 charge of each polymer, the charge density was calculated.

151 *Dynamic light scattering:* Dynamic light scattering (DLS) analysis (Malvern, Zetasizer Nano) was
152 carried out to assess the hydrodynamic radius (i.e., chain size: r_h , nm) of the three dispersants.

153

154 *2.2.2. Characterization of portlandite suspensions*

155 *Zeta potential:* To assess the electrokinetic interactions in the suspensions, the zeta potential (ζ
156 , mV) was determined by measurement of electrophoretic mobilities using Phase Analysis Light
157 Scattering (ZetaPALS, Brookhaven Instruments Corporation). The measurements were carried
158 out on dilute portlandite suspensions ($0.05 \text{ g}_{\text{solid}}/\text{L}_{\text{solution}}$) for a variety of dispersant dosages. In
159 select circumstances, before the zeta potential was measured, the pH of the suspensions was
160 adjusted to 12.8 and 13.0 by the addition of NaOH.

161

162 *Suspension rheology:* The rheological behavior of portlandite suspensions was assessed for a
163 range of particle volume fractions (ϕ) and dispersant dosages using a combined motor-
164 transducer rheometer (DHR-2, TA Instruments). A four-bladed vane-in-cup geometry was used,
165 with a vane of 28 mm diameter and 42 mm height, and a cup of 30 mm diameter. For all
166 measurements, the suspensions were conditioned to a temperature of $25 \text{ }^\circ\text{C} \pm 0.1 \text{ }^\circ\text{C}$. In
167 general, two types of analyses were carried out:

- 168 • The apparent yield stress (σ_y) and shear rate ($\dot{\gamma}$)-dependent viscosity (η) were determined
169 via a shear rate sweep. The apparent yield stress (σ_y) was identified as the stress plateau at
170 lower shear rates ($\dot{\gamma} < 1 \text{ s}^{-1}$).⁴⁰⁻⁴² Before the sweep, a 60 s pre-shear at $\dot{\gamma} = 100 \text{ s}^{-1}$ was
171 performed to remove any shear history effects, followed by a 60 s rest period.^{40,43,44}
172 Different rest periods of up to 180 s were tested during preliminary experiments with no
173 significant change (i.e., less than 15 % change in the peak stress stress) beyond 60 s of rest.
174 As the measured yield stress does not fully correspond to the *static yield stress* when no

Revised for Submission to Soft Matter (March 2020)

175 sufficient rest time is permitted for the suspension to rebuild its structure, therefore, the
176 term “*apparent yield stress*” was used herein. An ascending sweep was imposed in
177 logarithmically spaced steps (5 points per decade) from $\dot{\gamma} = 1 \times 10^{-3} \text{ s}^{-1}$ to 200 s^{-1} with a 10 s
178 data-averaging period. The ascending sweep was followed by a descending sweep over the
179 same shear rate range.

- 180 • The viscoelastic behavior and elasticity of aggregates in the suspensions were characterized
181 via small amplitude oscillatory (SAOS) rheometry. Following the shear flow experiment, a
182 shear-strain amplitude (γ) sweep from $\gamma = 0.001 \%$ to 1000% was performed, at a fixed
183 frequency of 1 Hz.

184

185 It should be noted that the rheological properties of portlandite suspensions were not affected
186 by potential carbonation of Ca(OH)_2 particles (i.e., the reaction of portlandite with atmospheric
187 CO_2 to produce solid calcium carbonates) over the course of rheology measurements. The initial
188 purity of Ca(OH)_2 used herein was as high as 95 % (very pure), and this amount did not change
189 over the course of the rheology experiment undertaken in atmospheric conditions ($[\text{CO}_2] = 0.04$
190 %). This was verified by comparing the carbonation extents of portlandite before and after
191 rheology measurements using thermogravimetric analysis (TGA; STA 6000, Perkin Elmer). Since
192 portlandite can rapidly carbonate in its near-surface vicinity (i.e., the first few nanometers),
193 TGA cannot offer definitive evidence that no surface carbonation occurred. Nevertheless,
194 however, the behavior of the portlandite suspensions was clearly distinguished from that of
195 calcite suspensions (not shown). More importantly, the portlandite particles did not show
196 differing atom density differences, i.e., at the near surface, and particle interior when observed
197 in backscatter imaging mode, or in the transmission electron microscope. This collective of
198 evidence suggests that the portlandite particles were not affected by (surficial) carbonation.

199

200 *Polymer adsorption:* The extent of polymer adsorption onto portlandite surfaces was
201 determined using a total organic carbon (TOC) analyzer (Shimadzu, TOC-L). Here, suspensions of
202 $\phi = 0.05$ with varying dispersant dosages up to 5 % by mass of solids (i.e., an upper bound on
203 dosage for typical applications) were composed and allowed to equilibrate for 24 h. Following
204 equilibration, the suspensions were then centrifuged for 15 min at 4696 rpm, and the
205 supernatant was removed and filtered using a $0.20 \mu\text{m}$ syringe filter. With all solid particles
206 removed, the amount of non-adsorbed polymer present was measured by TOC analysis. As the
207 inorganic carbon content may be elevated due to the formation of calcium carbonate (CaCO_3), a
208 non-purgeable organic carbon (NPOC) analysis was performed. Since the carbon content of
209 each of the dispersants was unknown, a calibration for each of the three dispersants was also
210 established by testing a series of known dilutions of dispersant up to a maximum dosage
211 equivalent to that found in the adsorption experiments. This allowed for a direct conversion to
212 be made between the NPOC content and dispersant dosage, which was unique for each
213 dispersant. The extent of polymer adsorption was then calculated using a mass balance with
214 the original amount of polymer added.

215

216 *Dynamic light scattering:* To assess the aggregation kinetics of suspensions for varying
217 dispersant types and dosages, dynamic light scattering (DLS) analysis (Malvern, Zetasizer Nano)
218 was carried out over time. Using dilute suspensions ($0.05 \text{ g}_{\text{solid}}/\text{L}_{\text{solution}}$) of portlandite in water,

Revised for Submission to Soft Matter (March 2020)

219 the Z-average size (intensity-based overall average size) of particle aggregates was determined
 220 by cumulants analysis (Malvern, Zetasizer Software). Each measurement was taken at around 5
 221 min intervals for up to 1 h with individual measurements requiring about 2 min each.

222

223 3. Results and Discussion

224 3.1 Aggregation, jamming, and yielding of portlandite suspensions

225 Portlandite particles suspended in a self-saturated or native solution (pH = 12.6) feature a zeta
 226 potential of $\zeta = +34$ mV (see Figure 1a). Typically, this magnitude of zeta potential is sufficient
 227 to impart electrostatic stability to a suspension.⁴⁵ However, electrostatic repulsion alone is
 228 unable to prevent particle aggregation and produce stable suspensions of portlandite. As such,
 229 portlandite suspensions demonstrated yield stresses that increase sharply with ϕ (see Figure
 230 1b) and a maximum achievable particle loading of $\phi_{max} \approx 0.36$. The ϕ_{max} was determined by
 231 fitting the yield stress- ϕ trends by a power-law function of the form $\sigma_y = (\phi_j - \phi)^m$,⁴⁶ where
 232 ϕ_j is the jamming volume fraction (analogous to ϕ_{max} in Krieger–Dougherty equation)⁴⁷ and m
 233 is a fitting exponent (see Figure 1b). It must be noted here that while suspensions of particles
 234 that offer long-range repulsion can exhibit significant yield stresses at low particle loading (e.g.,
 235 in suspensions comprising particles with thick adsorbed/grafted polymer layers that result in an
 236 expanded excluded volume around the particles)^{15,48}, the portlandite suspensions considered
 237 herein showed a high tendency for aggregation, which produced sharply increasing yield
 238 stresses, as discussed below.

239

240 An examination of the interparticle interactions reveals why, despite their high zeta potentials,
 241 portlandite suspensions are unstable. The (symmetric) interparticle interaction potential (V)
 242 between portlandite particles as a function of distance from the particle surface x (Equation 1)
 243 includes the contributions of electrostatic repulsion (V_{es}) that can be modeled using the Hogg-
 244 Healy-Fuerstenau⁴⁹ solution to the Poisson-Boltzmann equation, and van der Waals attraction (V_{vdW}),
 245 calculated using the nonretarded Hamaker pair potentials.^{50,51}

246

$V(x) = V_{es}(x) + V_{vdW}(x) = \pi\epsilon_r\epsilon_0\psi^2R \ln [1 + \exp(-\kappa x)] - \frac{AR}{12x}$	Equation 1
---	-------------------

247

248 Here, ϵ_r and ϵ_0 are the relative permittivity and permittivity of free space, respectively, and R is
 249 particle radius. The characteristic electrostatic decay length, or Debye length κ^{-1} was
 250 estimated as $\kappa^{-1} = \sqrt{\epsilon_r\epsilon_0kT/2e^2I}$, with k , T and e being the Boltzmann constant, temperature,
 251 and the elementary charge, respectively, and I being the ionic strength of the medium defined
 252 as $0.5\sum c_i z_i^2$ with c_i and z_i being the molar concentration and the valence of each ionic species
 253 present in the solution. For Ca(OH)₂ suspensions at their natural pH = 12.6, the ionic strength is
 254 60.9 mM, resulting in a Debye length $\kappa^{-1} = 1.2$ nm. The surface potential ψ was estimated from
 255 the measured zeta potential (ζ) of the particles at the shear plane ($x_s \sim \kappa^{-1}$)⁵² as $\psi = \zeta$
 256 $\exp(\kappa x_s)$. The Hamaker constant $A = 2.2 \times 10^{-20}$ J for Ca(OH)₂ was calculated following Lifshitz
 257 theory (see Supplementary Information: Section B, Equation S1).⁵³

258

Revised for Submission to Soft Matter (March 2020)

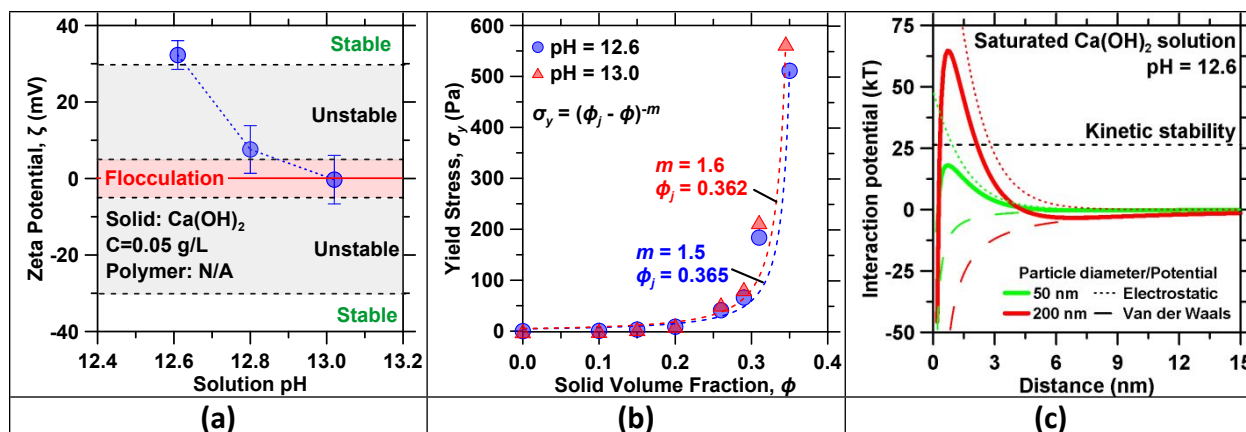


Figure 1: (a) Zeta potential ζ of Ca(OH)_2 particles as a function of pH in a saturated Ca(OH)_2 solution based on three replicate measurements. pH adjustments, as needed, were carried out by titrating with NaOH. The stable, unstable, and flocculation regions are included as reported elsewhere.^{54,55} (b) Ca(OH)_2 suspension's yield stress σ_y as a function of solid volume fraction ϕ at native pH (circles) and at the IEP (triangles) in the absence of any dispersant. Here, based on three replicate measurements, an uncertainty of 9 % in the yield stress and 5 % in fitting parameters was observed. The dashed lines indicate fits to the data with a power-law function of the form $\sigma_y = (\phi_j - \phi)^m$, where ϕ_j is the jamming volume fraction. (c) The calculated interparticle potentials based on electrostatic and van der Waals interactions for Ca(OH)_2 particles suspended in a saturated Ca(OH)_2 solution (pH 12.6).

259
 260 Figure 1c shows the total interparticle interaction potentials as well as the contributions from
 261 electrostatic and van der Waals interactions for 50 nm and 200 nm diameter portlandite
 262 particles. Strong screening of electrostatic interactions resulting from the compression of the
 263 electric double layer (EDL) that arises from the high ionic strength produces electrostatic
 264 repulsions for distances $x \lesssim 5$ nm. Short range van der Waals attraction dominates
 265 interparticle interactions at distances $x \lesssim 0.5$ nm. The resulting net interparticle interaction
 266 therefore transitions from a strong van der Waals attraction at $x \lesssim 0.5$ nm to an electrostatic
 267 repulsion in the range of $0.5 \text{ nm} \lesssim x \lesssim 5$ nm with a maximum around $x \sim 0.7$ nm and a weak
 268 van der Waals attraction for $x > 5$ nm, independent of particle size. The magnitude of the
 269 repulsive maximum is critical in determining the suspension's stability. The minimum energy of
 270 the repulsive barrier to prevent particle aggregation over a timescale τ can be estimated as
 271 $E_{min} = kT \ln(\tau f_c)$, where f_c is the collision frequency of particles under the influence of
 272 thermal forces (see Supplementary Information: Section C).⁵³ The kinetic criterion to maintain
 273 suspension stability over 24 h corresponds to $E_{min} = 25 \text{ kT} \pm 3 \text{ kT}$ for particles with a size on
 274 the order of 50 nm to 200 nm, as indicated by the horizontal dashed line in Figure 1c. In
 275 general, for portlandite particles smaller than 65 nm, the strength of the repulsive potential
 276 was found to be smaller than the kinetic barrier across all interparticle separations while for
 277 particles larger than 65 nm, interparticle repulsion was found to restrict interparticle approach
 278 only within distances smaller than ~ 3 nm. Thus, although the measured zeta potential of $\zeta = +$
 279 34 mV at pH = 12.6 is relatively high, high concentrations of counterions in the solution
 280 compress the EDL around the particles, thereby screening electrostatic repulsions very
 281 effectively. Consequently, the smaller primary portlandite particles (< 65 nm) are predicted to

Revised for Submission to Soft Matter (March 2020)

282 be unstable, and the larger particles (< 200 nm) are only stable at very small interparticle
283 spacings. Therefore, aggregation of portlandite particles for particle sizes < 200 nm is assured to
284 occur, thereby compromising the suspension's stability.

285
286 On account of their electrokinetic instability and tendency to aggregate, portlandite
287 suspensions display a sharp rise in yield stress at moderate particle loadings ($\phi = 0.2$; Figure 1b).
288 As such, solid volume fractions above $\phi_{max} = 0.36$ (see Figure 1b) were inaccessible in these
289 portlandite suspensions that have polydisperse plate-like particles in high ionic strength
290 aqueous environment. This is far inferior to the maximum achievable packing fraction, e.g. of
291 random close packings of monodisperse spheres ($\phi_{rcp} = 0.638$). Furthermore, the yielding
292 behavior of native suspensions (pH = 12.6) was largely analogous to the suspensions with their
293 pH regulated to the isoelectric point (IEP, $\text{pH}_{IEP} = 13$; Figure 1a), resulting in nearly identical
294 ϕ_{max} (see Figure 1b). At the IEP, electrostatic interactions between the particles are entirely
295 screened and only (attractive) van der Waals interactions operate, maximizing aggregation. The
296 similarity of the yield stress trends between the native portlandite suspensions and portlandite
297 suspensions at IEP with maximal aggregation indicates that particle aggregation is nearly
298 maximized at pH 12.6. Significantly, these observations confirm that zeta potentials cannot be
299 used as an indicator of stability for suspensions comprising strongly charged particles that
300 generate high concentrations of solubilized counterions. It should further be pointed out that
301 changing (reducing) the solution pH to increase the zeta potential of the particles is ineffective
302 for $\text{Ca}(\text{OH})_2$ particulates, as on account of their solubility and dissolution they self-regulate the
303 pH of their local environment. It is especially for these reasons that dispersant-induced
304 interactions are critical to control the rheology of portlandite (and other charged, soluble
305 particle) suspensions.

307 **3.2 Influences of dispersants on stability and rheology of portlandite suspensions**

308 Figure 2 displays the effects of dispersant addition for three dispersants including: a polyacrylic
309 acid-based linear polyelectrolyte dispersant (PAA), a lignosulfonate dispersant (LS), and a
310 polycarboxylate ether-based comb polyelectrolyte dispersant (PCE) composed of a polyacrylic
311 acid backbone and polyethylene glycol sidechains on the behavior of $\text{Ca}(\text{OH})_2$ suspensions. The
312 impact of dispersant on the suspension yield stress was found to vary significantly with
313 dispersant type (see Figure 2a). For example, at a constant solid volume fraction ($\phi = 0.35$), a
314 remarkable 10^5 -fold decrease in yield stress was achieved at a PCE dosage of 1.5 mass %
315 (polymer/solid). The reduction of the yield stress was found to increase exponentially with
316 increasing dispersant dosage ρ (% of solid); $\sigma_y/\sigma_{y,0} = \exp(-B\rho)$ where $\sigma_{y,0} = 663$ Pa (yield
317 stress of the $\phi = 0.35$ portlandite suspension with no dispersant). Here, B denotes the
318 efficiency of the dispersant in reducing the suspension yield stress; the effect of $B_{PCE} = 5.74$ in
319 an exponential function far exceeds those of $B_{PAA} = 2.06$ and $B_{LS} = 1.13$. The length scale and
320 strength of electrosteric repulsions provided by comb-like dispersants depend on the thickness
321 of the adsorbed layer, which in turn is dictated by the length, charge density, and stiffness of
322 the polyelectrolyte chain as well as the strength of the attractive electrostatic interactions
323 between the polyelectrolyte and the particles.^{14,39,56} Introduction of neutral side chains to the
324 polyelectrolyte backbone further enhances the efficacy of the dispersants.^{16,17,57} The neutral

Revised for Submission to Soft Matter (March 2020)

325 side chains in such ‘comb’ polyelectrolytes stretch out yet further away from the particle’s
 326 surface into the solvent, leading to higher particle dispersion.
 327

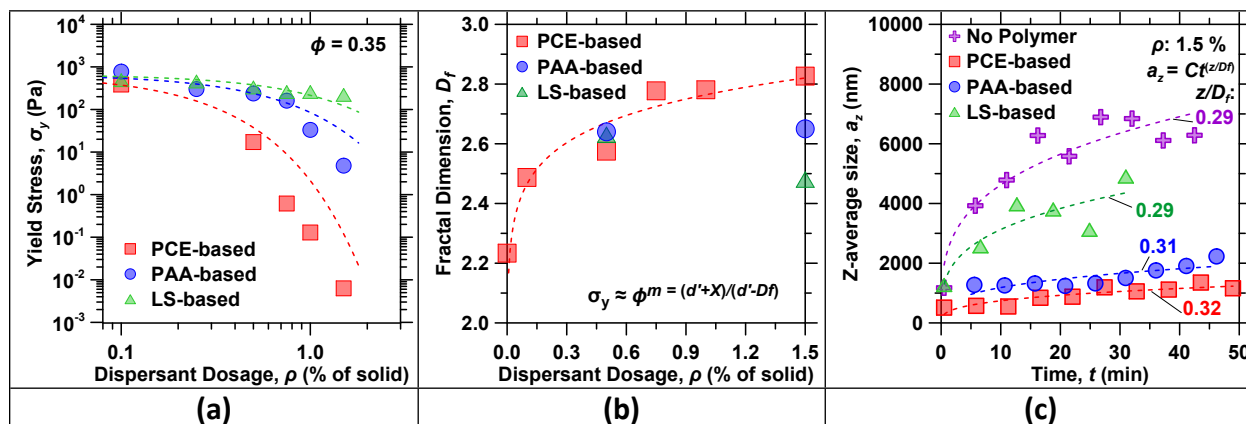


Figure 2: (a) The apparent yield stress of $\text{Ca}(\text{OH})_2$ suspensions σ_y as a function of dispersant dosage ρ for the three types of dispersants for $\phi = 0.35$. Here, based on 3 replicate measurements, the highest uncertainty of 9 % in the yield stress was observed. The dashed lines indicate exponential function fits to the data of the form $\sigma_y = \sigma_{y,0} \exp(-B\rho)$, with $\sigma_{y,0}$ and B being the yield stress of suspension without dispersants and a fitting parameter, respectively. (b) Fractal dimension D_f calculated from power-law scaling of yield stress vs. solid volume fraction for portlandite suspensions with various dispersant dosages and types. (c) The “Z-average” size of $\text{Ca}(\text{OH})_2$ aggregates as determined by DLS in suspensions composed at $\phi = 0.002$. These values are indicative of floc size; as $\text{Ca}(\text{OH})_2$ particles aggregate, the Z-average size increases. Based on 5 replicate measurements, the highest uncertainty of 20 % in the Z-average particle size was observed. The dashed lines indicate fits of the form $a_z = Ct^{z/D_f}$ to the data, where C and z are fitting parameters.

328
 329 Correspondent with a reduction in the yield stress with dispersant dosage at a fixed particle
 330 loading, the incorporation of dispersants also enhanced the maximum achievable particle
 331 volume fraction in the suspensions (see Supplementary Information: Figure S3). This
 332 enhancement is best shown by the addition of PCE to portlandite suspensions, wherein ϕ_{max}
 333 increased 1.4 times from 0.36 to 0.50 at a PCE dosage $\rho = 1.5\%$ of the solid mass (see
 334 Supplementary Information: Figure S3). The effects of PCE addition on the yield behavior of
 335 suspensions were examined over a range of volume fractions (see Supplementary Information:
 336 Figure S3). In the range of $0.1 < \phi < 0.5$, the addition of even modest amounts of PCE led to
 337 marked reductions in the yield stress. The influence of adding dispersants could further be
 338 quantified by deducing the fractal dimension of the flocs forming in the suspensions (see Figure
 339 2b). The fractal dimension D_f was extracted from power-law fits of the form $\sigma_y \sim \phi_s^m$ where $m =$
 340 $\frac{D+X}{D-D_f}$. Here, D is the Euclidean dimension (3, for a 3D space), D_f is the fractal dimension of
 341 particle clusters, and X is the fractal dimension of the cluster backbones, taken as 1 indicative
 342 of a backbone that’s not capable of elastic stress transmission (see Supporting Information:
 343 Sections E and F).⁵⁸ The yield stress σ_y of the portlandite suspension with no dispersant
 344 indicated a power-law scaling $m \approx 5.2$ (see Supplementary Information, Figure S3), consistent

Revised for Submission to Soft Matter (March 2020)

345 with the observed yield stress behavior of aggregating suspensions of mineral particles.⁵⁹ A
346 steady increase in the fractal dimension (i.e., approaching 3 for a sphere) of the suspensions
347 with PCE dosage (see Figure 2b) signified that suspension structure shifts further away from the
348 diffusion-limited aggregation regime on account of enhanced steric barriers that retard
349 aggregation upon addition of PCE to the suspensions. This results in a structural transition from
350 more branched flocs (i.e., more open structure) to either denser flocs or greater particle
351 dispersion. This transition occurs when the forces mitigating aggregation grow greater and
352 particle sticking/collision efficiency resulting from diffusing clusters decreases. This permits an
353 increase in the maximum achievable particle volume fraction. It should be noted that
354 depending on the suspension structure, the increase in the value of the fractal dimension can
355 be an indicative of two different cases: (i) individual flocs are approaching more ideal packing
356 into a spherical shape, which can be accomplished by forming more densely-packed flocs, or (ii)
357 stronger particle dispersion, whereby flocs are made up of few primary particles.^{58,60} As the
358 reduction in yield stress is much greater for suspensions made with the comb-like dispersant, it
359 is inferred that any flocs formed in these suspensions are much smaller with weaker linkages
360 than that of the native portlandite suspension and those made with linear dispersants (see
361 Supplementary Information: Figure S4).

362
363 The reduction in yield stress upon the addition of the dispersants corresponds to restricted
364 aggregate sizes and retarded aggregate growth. The temporal evolution of aggregate size using
365 dynamic light scattering measurements in very dilute portlandite suspensions highlighted the
366 close correlation between the efficacy of dispersants in reducing yield stress and inhibiting
367 aggregate growth. In general, the addition of PCE, which most reduced yield stresses, resulted
368 in the smallest and slowest-growing $\text{Ca}(\text{OH})_2$ aggregates. Whereas the addition of LS, which
369 resulted in only marginally smaller suspensions yield stresses, led to only minor reductions in
370 both aggregate sizes and growth rates as compared to the native $\text{Ca}(\text{OH})_2$ suspension (see
371 Figure 2c). Although the size evolution of PCE and PAA was similar, the marked difference in the
372 effect on yield stress results from the greater ability of PCE to provide a steric barrier between
373 particles. While both dispersants are effective at reducing the overall size of aggregates, PAA
374 does not keep the smaller aggregates spaced apart, leading to smaller interparticle spacing and
375 higher rheological properties. The addition of dispersants also led to weaker aggregates, such
376 that the reduction of suspension yield stress with dispersant type and dosage correlated closely
377 with lower strains and the energy required to disrupt the overall suspension's structure (see
378 Supplementary Information: Figure S4). Despite similar floc size for PCE and PAA dispersants,
379 weaker linkages between flocs/aggregates were noted for the comb polyelectrolyte PCE
380 dispersant due to its steric hindrance.

381
382 The elucidation of aggregate growth kinetics enables further insights into the nature of the
383 aggregation processes. The mean aggregate size a_z for aggregates should grow with time t as a_z
384 $= Ct^{z/D_f}$, where C is a numerical prefactor and z is related to the nature of the aggregation
385 processes. For diffusion limited aggregation, $z = 1$ and $D_f = 1.75-1.8$, resulting in $a_z \sim t^{0.55}$.
386 For reaction limited aggregates, $D_f \geq 2.1$ and z is generally smaller than 1, resulting in the
387 temporal power-law exponent (z/D_f) generally being < 0.45 .⁶¹ The temporal power-law

Revised for Submission to Soft Matter (March 2020)

388 exponent of aggregate growth in Ca(OH)₂ suspensions, both with and without dispersants, was
 389 found to be smaller than 0.4, pointing towards reaction limited aggregation of Ca(OH)₂
 390 particles. Using D_f data from Figure 2b, z values were determined to be smaller than 1 ($z_{none} =$
 391 0.65, $z_{LS} = 0.72$, $z_{PAA} = 0.82$, and $z_{PCE} = 0.91$), highlighting the prominent contribution of the
 392 sticking of smaller clusters in the aggregation process.⁶¹ The values of C ($C_{none} = 2372$, $C_{LS} =$
 393 1593, $C_{PAA} = 582$, and $C_{PCE} = 355$) corresponded to the effectiveness of each dispersant in
 394 reducing aggregation in the suspensions and correlated well with the fitting parameter B (see
 395 Figure 2a), highlighting the reduced propensity towards aggregation induced by the addition of
 396 dispersants. To further analyze the aggregation kinetics via Smoluchowski's model⁶², the floc
 397 size evolution in Figure 2c was used to assess the rate of increase in the number of particles N_i
 398 in time t within a floc by $N_i \approx \left(\frac{R_{floci}}{a}\right)^{D_f} 63$, where R_{floci} is the floc size at time t (using data from
 399 Figure 2c) and a is the primary particle size. The aggregation rate constant via colliding particles
 400 with time k_a was determined by fitting the N_i/N_0 -time trends by a linear function of the form
 401 $N_i/N_0 = k_a t$. The normalized particle number N_i/N_0 within floc was obtained by particle
 402 number N_i at time t to its initial reading N_0 . The k_a values were found to be substantially
 403 smaller than that the neat portlandite suspension ($k_{a,none} = 0.023 \text{ s}^{-1}$, $k_{a,LS} = 0.013 \text{ s}^{-1}$, $k_{a,PAA} =$
 404 0.006 s^{-1} , and $k_{a,PCE} = 0.004 \text{ s}^{-1}$). This reveals that the addition of dispersant, especially PCE,
 405 significantly reduces particle sticking and collision efficiency as well as retards aggregation
 406 growth greatly. Herein, it should be noted that the solvent's viscosity increases only marginally,
 407 owing to the presence of non-adsorbed dispersant in the solvent. As such, the reduced rate of
 408 aggregation for suspensions with dispersant is not due to reduced particle collisions, e.g.,
 409 arising from possible increases in solvent viscosity, but due to the increased interparticle
 410 repulsions that are induced by the dispersant. It should be noted that the free dispersant in the
 411 solvent may have other impacts such as attractive depletion in addition to altering solvent
 412 viscosity. However, the contribution of attraction depletion to particle bridging/flocculation and
 413 the consequent change (increase) in rheological properties of suspension is expected to be
 414 marginal due to the relatively low molecular weights of the backbone of dispersants
 415 investigated herein. As the floc size for suspensions made with dispersants at the highest
 416 dosage ($\rho = 1.5 \%$ of the solid mass) remained smaller than that of the native portlandite
 417 suspension (as evidenced by DLS data in Figure 2c), it is inferred that free dispersant in solvent
 418 does not result in polymer bridging induced flocculation of particles.

419
 420 A quantification of dispersant adsorption on particle surfaces was pursued to link the dispersant
 421 affinity to the observed yield stress reductions. The relationship between the amount of
 422 adsorbed dispersant, ρ_a and free dispersant, ρ_f , is depicted in Figure 3a and was described by
 423 a Langmuir adsorption isotherm of the form: $\frac{\rho_a}{\rho_{a,m}} = \frac{\rho_f K}{1 + \rho_f K}$.^{54,64} A plateau in the amount of
 424 adsorbed dispersant $\rho_{a,m}$ with increasing ρ_f was recognized and the equilibrium constant K ,
 425 which describes the ease and tendency of polymer adsorption onto the portlandite surfaces,
 426 was obtained (Table 1). It should be noted that (i) adsorption behavior was only examined in a
 427 range that is expected to be relevant for typical applications, i.e., $\rho \leq 5 \%$ [N.B.: It is important
 428 to limit the dispersant dosages to restrict the abundance of free polymer in solution, which

Revised for Submission to Soft Matter (March 2020)

429 could otherwise induce substantial attractive depletion forces], and (ii) the assumption in the
 430 Langmuir adsorption model of *on-average* monolayer adsorption is expected to be reasonable
 431 for the dosages considered herein although multilayer adsorption may occur at higher
 432 dispersant concentrations.^{14,21,65}
 433

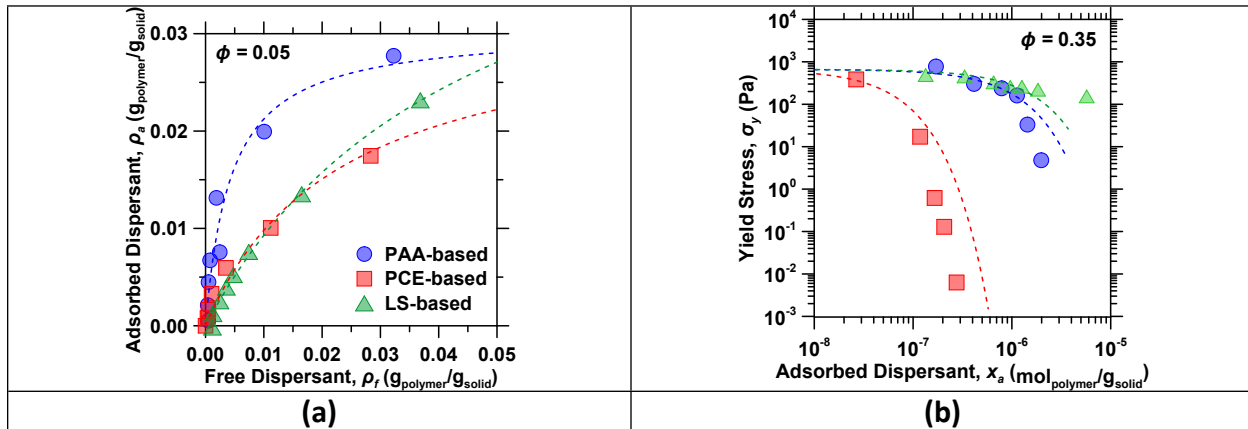


Figure 3: (a) The amount of dispersant adsorbed onto portlandite particles surfaces ρ_a as a function of the free dispersant concentration in solution ρ_f . The dashed lines indicate fits to the data with a Langmuir expression for monolayer adsorption. (b) The yield stress σ_y of portlandite suspensions as a function of the moles of dispersant adsorbed on the particle surfaces per unit mass of the solids x_a . The dashed lines indicate exponential function fits to the data of the form $\sigma_y = \sigma_{y,0} \exp(-Dx_a)$, where $\sigma_{y,0} = 663$ Pa (yield stress of the $\phi = 0.35$ portlandite suspension with no dispersant) and D is a fitting parameter. Here, based on 5 replicates, the highest uncertainty of 10 % in the amount of dispersant adsorbed, was noted.

434
 435 The polymer charge density, molecular weight, and length of side chains all contribute towards
 436 the binding affinity K , where higher charge densities, larger molecular weights, and smaller
 437 persistence lengths should result in higher values of K . The linear and densely charged PAA
 438 dispersants adsorbed readily onto the particle surfaces, providing steric exclusion to the
 439 particles while retaining high adsorption. The lower binding affinity of the LS chains is
 440 hypothesized to result from the aromatic rings within its structure, which reduces its flexibility,
 441 thus entropically limiting adsorption due to the lack of favorable conformations. The lower
 442 binding affinity of PCE chains can be attributed to the specific molecular structure. Even though
 443 the PCE has the largest molecular weight amongst all the three dispersants (~ 39.5 kDa), a
 444 majority of it (~ 32.5 kDa) is contributed by the neutral polyethylene glycol sidechains (see
 445 Supplementary Information: Section H). The polyacrylic acid backbone accounts for around 7
 446 kDa of the total molecular weight and is expected to be ~ 50 % less charge dense than linear
 447 PAA chains. The presence of side chains would also reduce the conformational entropy of the
 448 PCE chains. The combined impact of lower charge density and conformation entropy of the
 449 polyacrylic acid backbone on adsorption translates to a significant decrease in the binding
 450 affinity of the PCE chains.^{21,66}
 451

Table 1: Properties and adsorption characteristics of the investigated dispersants.

Revised for Submission to Soft Matter (March 2020)

Dispersant Type	Mass-average molecular weight, M_W (g/mol)	Charge density at pH = 12 (eq/mol)	Hydrodynamic radius, r_H (nm)	Adsorption capacity, $\rho_{a,m}$ (g _{polymer} /g _{solid})	Binding affinity, K (~)
PCE	39,467	43.5	11.34	0.0325	43.32
PAA	6,092	81.0	4.45	0.0305	229.7
LS	4,050	8.4	2.61	0.0520	21.75

452
 453 The efficacy of the dispersants is highlighted by examining the yield stress reductions plotted as
 454 a function of the mole fraction of adsorbed dispersant (see Figure 3b). When normalized by
 455 mole fraction, the difference in the efficacies of PCE and other dispersants in reducing the yield
 456 stress becomes even more drastic. In effect, even with low binding affinity and at very small
 457 dosages, the polyethylene glycol side chains of the adsorbed PCE polymers stretch into the
 458 solvent and provide strong screening of the attractive van der Waals forces. The linear PAA and
 459 LS dispersants show similar behavior at low levels of adsorption, forming an adsorbed layer on
 460 the surface whose thickness increases with increasing polymer content. LS shows a saturation
 461 in affecting yield behavior while the effectiveness of PAA improves above an adsorption level
 462 around 10^{-6} mol_{polymer}/g_{solid}. This can be attributed to a sharp increase in the dispersant layer
 463 thickness after the particle surfaces are saturated with polymer, owing to the higher PAA
 464 charge density. The marked difference in the effectiveness of linear and comb polyelectrolyte
 465 dispersants, however, highlights the role of side chains in providing an effective steric barrier to
 466 particle aggregation. Furthermore, while larger linear polyelectrolytes facilitate aggregation due
 467 to overlap of the adsorbed polyelectrolyte layers and resulting particle bridging,^{67,68} increasing
 468 the molecular weight of comb polyelectrolytes in fact facilitates dispersion. This is due to the
 469 increased adsorbed polymer layer thickness, owing to the enhanced steric repulsion between
 470 the overlapping neutral sidechains.

471
 472 The influence of the dispersants on altering interparticle separations was assessed, to a first
 473 approximation, by estimating the average surface-to-surface separation amongst particles
 474 based on knowledge of their solid volume fraction in the suspension and the particle size
 475 distribution (see Supplementary Information Section D). Figure 4a shows a simplified trace for
 476 the native portlandite suspension's yield stress as a function of the interparticle spacing d_p for a
 477 range of particle volume fractions; $0.10 \leq \phi \leq 0.35$. This relationship offers a simple means to
 478 establish the correlation between changes in the yield stress σ_y and the average interparticle
 479 spacing d_p . This correlation was used to map the effective increase in the interparticle distance
 480 that is produced by the addition of dispersants (see Figure 4a). The outcomes of this analysis,
 481 plotted as $|\Delta d_p / \Delta \sigma_y|$ as a function of the amount of adsorbed polymer ρ_a in Figure 4b, indicate
 482 that the differing ability of the dispersants to reduce the suspension's yield stress is intrinsically
 483 related to their ability to induce controllable separations between particles as a function of
 484 their adsorption behavior.

485

Revised for Submission to Soft Matter (March 2020)

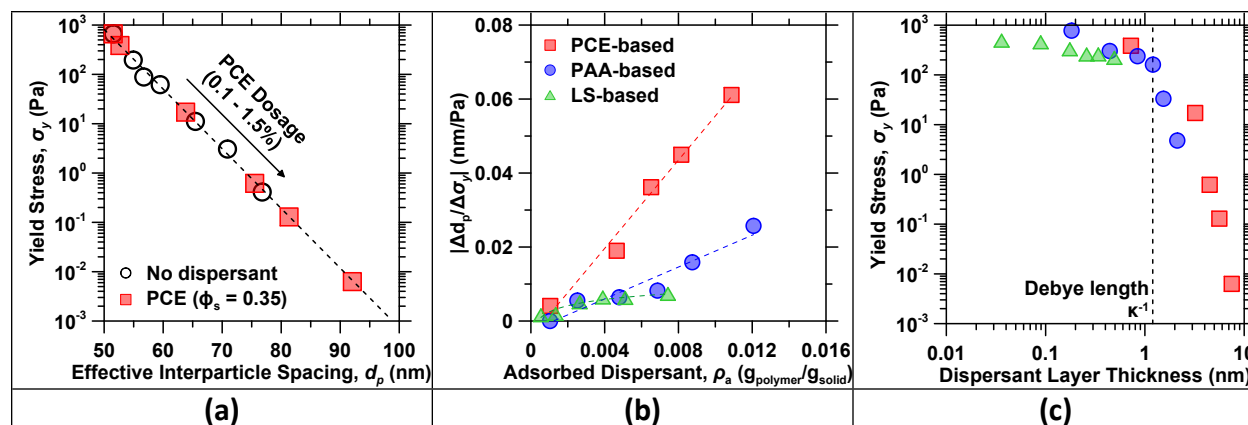


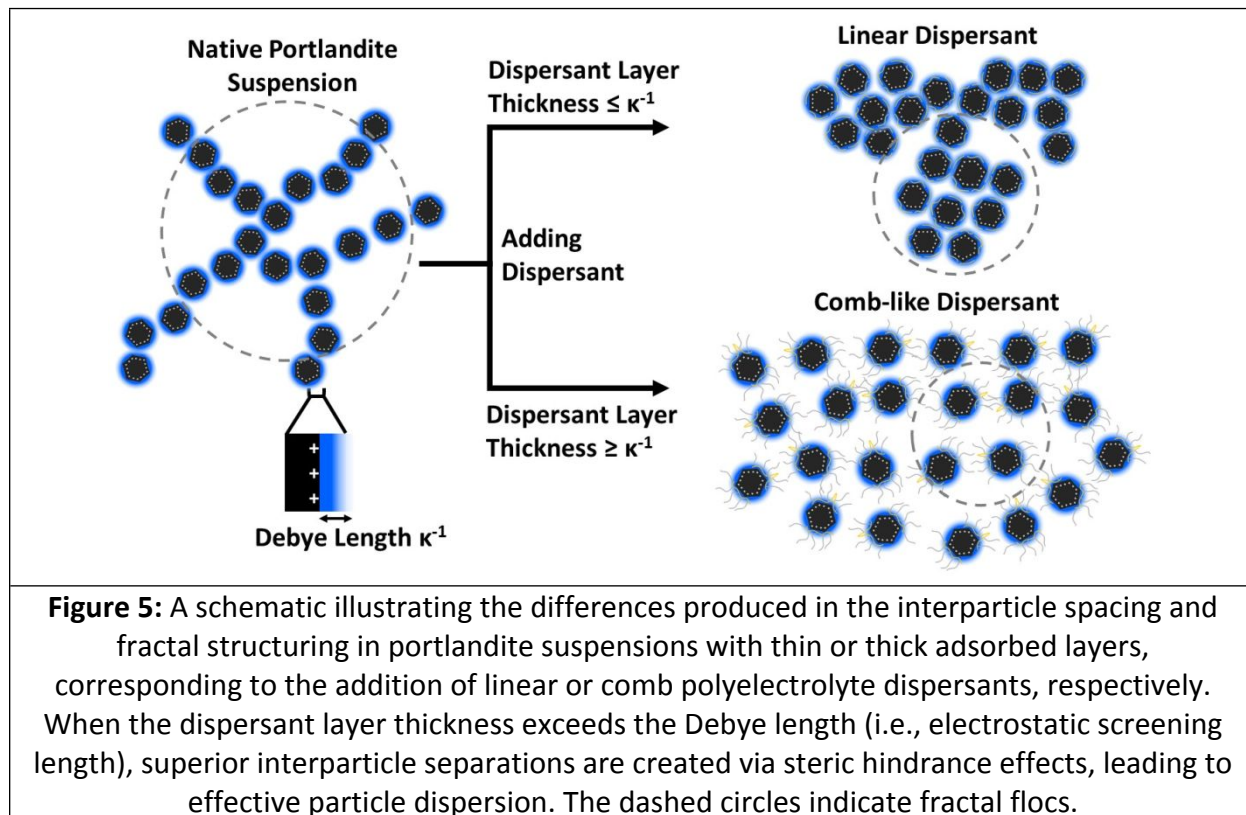
Figure 4: (a) The suspension's yield stress σ_y as a function of interparticle (surface-to-surface) separation d_p for the native portlandite suspension. By mapping the measured yield stress to the interparticle spacing, the effect of a given dispersant on reducing the yield stress at a specific dosage can be established. (b) Continuation of analysis in (a) showing the reduction in yield stress as the effective interparticle spacing increases for the different polymers. (c) The apparent yield stress as a function of an effective dispersant layer thickness for all the polymers. In general, it is seen that the yield stress reduces by nearly 5 orders of magnitude as the dispersant layer thickness progressively exceeds the electrostatic screening length.

486

487 The ability to induce controlled interparticle separations is a function of electrosteric behavior,
 488 especially in high ionic strength suspensions. A relevant attribute of dispersant in such cases is
 489 its hydrodynamic radius (r_H , see Table 1). The hydrodynamic radius describes the physical size
 490 of a polymer molecule in a solution. Although r_H does not perfectly describe the conformation
 491 of the adsorbed polymer, it offers an estimate of the interaction distance for steric repulsion of
 492 each dispersant. Thus, the effectiveness of each dispersant, i.e., the dispersant layer thickness,
 493 can be described by the product of its fractional amount adsorbed (i.e., surface coverage, $\rho_a /$
 494 $\rho_{a,m}$) and its hydrodynamic radius. Figure 4c reveals a remarkable mapping between suspension
 495 yield stresses and estimated dispersant layer thickness ($r_H \rho_a / \rho_{a,m}$), with data for all three
 496 dispersants collapsing onto a single "master" curve. In addition, it is noted that a sharp
 497 reduction of nearly five orders of magnitude in the yield stress is produced when the dispersant
 498 layer thickness exceeds the electrostatic screening length (i.e., Debye length, κ^{-1}). This
 499 observation indicates that, in general, the most prominent attribute of a dispersant is to offer a
 500 sufficient dispersant layer thickness that induces physical separation amongst particles over a
 501 length scale greater than that over which Coulombic forces would operate, as schematically
 502 illustrated in Figure 5. The interparticle interactions produced by adsorbed polymers are
 503 controlled by their structure. Since the LS and PAA dispersants do not feature branched or
 504 grafted side chains, they cannot present sufficiently thick adsorbed layers, and consequently,
 505 do not impose significant interparticle steric repulsion. Furthermore, we acknowledge that r_H
 506 for strongly charged polymers (e.g., PAA) will be influenced by chain swelling, owing to intra-
 507 chain electrostatic repulsion. Importantly, the swollen conformation should translate to thicker
 508 adsorbed polymer layers, again owing to intra-chain repulsion of the non-adsorbed sections of
 509 the chains. Taken together, since the PCE is the only dispersant examined herein that is capable

Revised for Submission to Soft Matter (March 2020)

510 of producing a substantial dispersant layer thickness (e.g., as indicated by its comb architecture,
 511 high molecular weight, and r_H) that exceeds the electrostatic screening length, it is the only
 512 dispersant that is effective at creating larger particle separations, mitigating particle
 513 aggregation, and reducing the yield stress of nano- and micro-scale portlandite suspensions.
 514



515
 516 **4. Summary and conclusions**
 517 This study has elucidated the impact of polymers that present different dispersion mechanisms
 518 (i.e., electrostatic and electrosteric) on the stability and rheological properties of portlandite
 519 suspensions that present short screening lengths and a native pH close to the particle's
 520 isoelectric point (pH \approx 12.6, IEP: pH \approx 13). Special attention was paid to link the characteristics
 521 of dispersants to the suspension's yield behavior. High ionic strengths disrupt electrostatic
 522 repulsion by screening charges and induce particle aggregation, resulting in a significant
 523 increase in yield stress and consequently lowering the maximum achievable solid volume
 524 fraction (ϕ_{max}) in native portlandite suspensions. Thus, it was indicated that simple Coulombic
 525 repulsion alone is insufficient to affect the rheology of native portlandite suspensions. A
 526 stronger screening of the interparticle attractive van der Waals forces was introduced via
 527 longer-range geometrical particle-particle exclusion by adding polyelectrolyte dispersants that
 528 adsorb on particle surfaces and provide steric hindrance, limiting particle aggregation. The
 529 ability of dispersants to induce interparticle separation was found to be dominantly controlled
 530 by the dispersant layer thickness, and how far it extends into the solvent. Specifically, when the
 531 (adsorbed) dispersant layer thickness exceeded the electrostatic screening length in high ionic
 532 strength solutions, it imparted interparticle separation via steric hindrance. Thus, a "comb"

Revised for Submission to Soft Matter (March 2020)

533 polyelectrolyte PCE dispersant was nearly 5x more effective at reducing the yield stress of
534 portlandite suspensions as compared to linear dispersants at similar portlandite volume
535 fractions. The analyses highlighted that although the total molecular weight (M_w) is an
536 important characteristic that is indicative of dispersant effectiveness, the molecular weight of
537 the side chains and the hydrodynamic radius are in fact more relevant attributes influencing
538 interparticle separations and aggregation. The understanding gained from this study offers
539 broad insights into the design of more effective dispersants for controlling interparticle
540 separations in suspensions that self-regulate their pH and present short electrostatic screening
541 lengths. This knowledge is fundamental to control the rheological behavior and maximum
542 achievable solid volume fraction of dense suspensions to ensure relevant engineering scale-
543 processability.

544

545 **Acknowledgements**

546 The authors acknowledge financial support for this research from the National Science
547 Foundation (DMREF: 1922167, CMMI: 1562066, CAREER: 1253269), Department of Energy:
548 Office of Fossil Energy via the National Energy Technology Laboratory (NETL; DE-FE0029825 and
549 DE-FE0031718), and TRANSCEND: A joint UCLA-NIST Consortium that is funded by its industry
550 and agency partners. This research was conducted in the Laboratory for the Chemistry of
551 Construction Materials (LC²) and the Electron Microscopy Core Facility at UCLA. The authors
552 gratefully acknowledge the support provided by these laboratories. The authors thank BASF
553 Corporation: Construction Chemicals (Beachwood, Ohio) for their assistance in polymer
554 characterization. The contents of this paper reflect the views and opinions of the authors, who
555 are responsible for the accuracy of the datasets presented herein, and do not reflect the views
556 and/or policies of the funding agencies, nor do the contents constitute a specification, standard
557 or regulation.

558

559 **Supporting Information**

560 Particle size distribution, Fourier Transform Infrared Spectroscopy, Lifshitz Theory for
561 Calculation of the Hamaker Constant, Kinetic Stability Criterion, Yield stress Behavior for PCE-
562 containing Suspensions, Fractal Dimension of Aggregates, Crossover Energy, Nuclear Magnetic
563 Resonance Characterization.

564

565 **Conflicts of Interest**

566 There are no conflicts to declare.

567

568 **References**

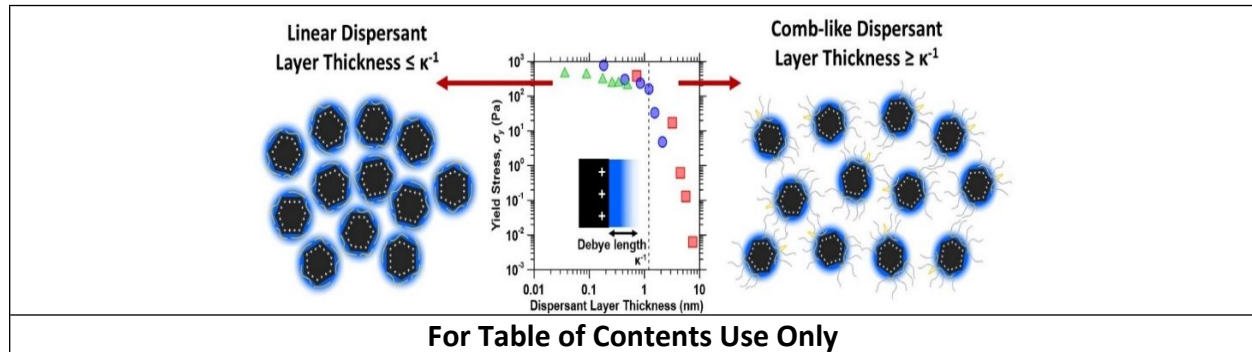
- 569 1 N. Roussel, *Understanding the Rheology of Concrete*, Elsevier, 2011.
- 570 2 P. F. G. Banfill, in *Proceedings of the 11th international cement chemistry congress*, 2003, vol. 1, pp.
571 50–62.
- 572 3 X. Liu, Y. Huang and J. Yang, *Ceramics International*, 2002, **28**, 159–164.
- 573 4 S. B. Johnson, D. E. Dunstan and G. V. Franks, *Journal of the American Ceramic Society*, 2002, **85**,
574 1699–1705.
- 575 5 A. Vintiloiu and J.-C. Leroux, *Journal of Controlled Release*, 2008, **125**, 179–192.
- 576 6 M. Zignani, C. Tabatabay and R. Gurny, *Advanced Drug Delivery Reviews*, 1995, **16**, 51–60.

Revised for Submission to Soft Matter (March 2020)

- 577 7 W. Bauer and D. Nötzel, *Ceramics International*, 2014, **40**, 4591–4598.
578 8 S. Mubeen, Y. Jun, J. Lee and E. W. McFarland, *ACS Appl. Mater. Interfaces*, 2016, **8**, 1759–1765.
579 9 D. Lowke, E. Dini, A. Perrot, D. Weger, C. Gehlen and B. Dillenburger, *Cement and Concrete Research*,
580 2018, **112**, 50–65.
581 10 X. Ren, H. Shao, T. Lin and H. Zheng, *Materials & Design*, 2016, **101**, 80–87.
582 11 E. Ruiz-Agudo and C. Rodriguez-Navarro, *Langmuir*, 2010, **26**, 3868–3877.
583 12 M. Fourmentin, G. Ovarlez, P. Faure, U. Peter, D. Lesueur, D. Daviller and P. Coussot, *Rheol Acta*,
584 2015, **54**, 647–656.
585 13 W. B. Russel, D. A. Saville and W. R. Schowalter, *Colloidal dispersions*, Cambridge university press,
586 1991.
587 14 A. Zingg, F. Winnefeld, L. Holzer, J. Pakusch, S. Becker and L. Gauckler, *Journal of Colloid and Interface*
588 *Science*, 2008, **323**, 301–312.
589 15 S. Srivastava, J. H. Shin and L. A. Archer, *Soft Matter*, 2012, **8**, 4097–4108.
590 16 H. Kamiya, Y. Fukuda, Y. Suzuki, M. Tsukada, T. Kakui and M. Naito, *Journal of the American Ceramic*
591 *Society*, 1999, **82**, 3407–3412.
592 17 A. Pettersson, G. Marino, A. Pursiheimo and J. B. Rosenholm, *Journal of Colloid and Interface Science*,
593 2000, **228**, 73–81.
594 18 Y. Leong, D. V. Boger and D. Parris, *Journal of Rheology*, 1991, **35**, 149–165.
595 19 P. F. Luckham and J. Klein, *Journal of the Chemical Society, Faraday Transactions 1: Physical Chemistry*
596 *in Condensed Phases*, 1984, **80**, 865–878.
597 20 Y. De Hazan, J. Heinecke, A. Weber and T. Graule, *Journal of Colloid and Interface Science*, 2009, **337**,
598 66–74.
599 21 G. H. Kirby and J. A. Lewis, *Journal of the American Ceramic Society*, 2004, **87**, 1643–1652.
600 22 S. Dean, C.-T. Chen, L. Struble and H. Zhang, *J. ASTM Int.*, 2006, **3**, 12787.
601 23 M. Mirnezami, L. Restrepo and J. A. Finch, *Journal of Colloid and Interface Science*, 2003, **259**, 36–42.
602 24 T. Sowoidnich, T. Rachowski, C. Rößler, A. Völkel and H.-M. Ludwig, *Cement and Concrete Research*,
603 2015, **73**, 42–50.
604 25 J. Plank and B. Sachsenhauser, *Cement and Concrete Research*, 2009, **39**, 1–5.
605 26 R. G. Bates, V. E. Bower and E. R. Smith, *Journal of Research of the National Bureau of Standards*,
606 1956, **56**, 305–312.
607 27 T. P. Murphy, E. E. Prepas, J. T. Lim, J. M. Crosby and D. T. Walty, *Lake and Reservoir Management*,
608 1990, **6**, 101–108.
609 28 S. Lim, W. Jeon, J. Lee, K. Lee and N. Kim, *Water Research*, 2002, **36**, 4177–4184.
610 29 Q. Chen, Z. Luo, C. Hills, G. Xue and M. Tyrer, *Water Research*, 2009, **43**, 2605–2614.
611 30 B. Rosenberg, P. E. Murray and K. Namerow, *Dental Traumatology*, 2007, **23**, 26–29.
612 31 C. Sathorn, P. Parashos and H. Messer, *International Endodontic Journal*, 2007, **40**, 2–10.
613 32 U. SJÖGREN, D. Figdor, L. Spångberg and G. Sundqvist, *International Endodontic Journal*, 1991, **24**,
614 119–125.
615 33 F. Martínez-Bustos, Y. K. Chang, A. C. Bannwart, M. E. Rodríguez, P. A. Guedes and E. R. Gaiotti, *Cereal*
616 *Chemistry*, 1998, **75**, 796–801.
617 34 L. Han, Z. Lu, X. Hao, Y. Cheng and L. Li, *Journal of Texture Studies*, 2012, **43**, 227–234.
618 35 C. Rodriguez-Navarro, E. Hansen and W. S. Ginell, *Journal of the American Ceramic Society*, 1998, **81**,
619 3032–3034.
620 36 O. Cazalla, C. Rodriguez-Navarro, E. Sebastian, G. Cultrone and M. J. D. la Torre, *Journal of the*
621 *American Ceramic Society*, 2000, **83**, 1070–1076.
622 37 D. R. Lide, *CRC Handbook of Chemistry and Physics, 85th Edition*, CRC Press, 2004.
623 38 Q. Shen, T. Zhang and M.-F. Zhu, *Colloids and Surfaces A: Physicochemical and Engineering Aspects*,
624 2008, **320**, 57–60.

Revised for Submission to Soft Matter (March 2020)

- 625 39 L. M. Rueschhoff, J. P. Youngblood and R. W. Trice, *Journal of the American Ceramic Society*, 2016, **99**,
626 3857–3865.
- 627 40 K. Vance, G. Sant and N. Neithalath, *Cement and Concrete Composites*, 2015, **59**, 38–48.
- 628 41 Q. D. Nguyen and D. V. Boger, *Annual Review of Fluid Mechanics*, 1992, **24**, 47–88.
- 629 42 P. R. de Souza Mendes and R. L. Thompson, *Rheologica Acta*, 2013, **52**, 673–694.
- 630 43 S. A. Nair, H. Alghamdi, A. Arora, I. Mehdipour, G. Sant and N. Neithalath, *Journal of the American*
631 *Ceramic Society*, 2019, **102**, 3951–3964.
- 632 44 F. Khalkhal, P. J. Carreau and G. Ausias, *Journal of rheology*, 2011, **55**, 153–175.
- 633 45 M. Wiśniewska, *Powder Technology*, 2010, **198**, 258–266.
- 634 46 E. Brown and H. M. Jaeger, *Physical review letters*, 2009, **103**, 086001.
- 635 47 I. M. Krieger and T. J. Dougherty, *Transactions of the Society of Rheology*, 1959, **3**, 137–152.
- 636 48 A. R. Studart, E. Amstad and L. J. Gauckler, *Langmuir*, 2007, **23**, 1081–1090.
- 637 49 R. Hogg, T. W. Healy and D. W. Fuerstenau, *Transactions of the Faraday Society*, 1966, **62**, 1638–
638 1651.
- 639 50 H. C. Hamaker, *Physica*, 1937, **4**, 1058–1072.
- 640 51 U. Aschauer, O. Burgos-Montes, R. Moreno and P. Bowen, *Journal of Dispersion Science and*
641 *Technology*, 2011, **32**, 470–479.
- 642 52 W. Ding, X. Liu, L. Song, Q. Li, Q. Zhu, H. Zhu, F. Hu, Y. Luo, L. Zhu and H. Li, *Surface Science*, 2015, **632**,
643 50–59.
- 644 53 J. N. Israelachvili, *Intermolecular and Surface Forces*, Academic Press, 2015.
- 645 54 K. Yoshioka, E. Tazawa, K. Kawai and T. Enohata, *Cement and Concrete Research*, 2002, **32**, 1507–
646 1513.
- 647 55 S. Hornig and T. Heinze, *Biomacromolecules*, 2008, **9**, 1487–1492.
- 648 56 F. Winnefeld, S. Becker, J. Pakusch and T. Götz, *Cement and Concrete Composites*, 2007, **29**, 251–262.
- 649 57 K. Yoshioka, E. Sakai, M. Daimon and A. Kitahara, *Journal of the American Ceramic Society*, 1997, **80**,
650 2667–2671.
- 651 58 W.-H. Shih, W. Y. Shih, S.-I. Kim, J. Liu and I. A. Aksay, *Phys. Rev. A*, 1990, **42**, 4772–4779.
- 652 59 D. V. Boger, *Annual Review of Chemical and Biomolecular Engineering*, 2013, **4**, 239–257.
- 653 60 T. Liberto, M. Le Merrer, C. Barentin, M. Bellotto and J. Colombani, *Soft matter*, 2017, **13**, 2014–2023.
- 654 61 L. T. Trinh, A.-L. Kjøniksen, K. Zhu, K. D. Knudsen, S. Volden, W. R. Glomm and B. Nyström, *Colloid and*
655 *Polymer Science*, 2009, **287**, 1391.
- 656 62 M. Von Smoluchowski, *Phys. Z. Sowjet.*, 1916, **17**, 557–571.
- 657 63 D. B. Genovese, *Advances in colloid and interface science*, 2012, **171**, 1–16.
- 658 64 F. Khalkhal, A. S. Negi, J. Harrison, C. D. Stokes, D. L. Morgan and C. O. Osuji, *Langmuir*, 2018, **34**,
659 1092–1099.
- 660 65 F. Dalas, A. Nonat, S. Pouchet, M. Mosquet, D. Rinaldi and S. Sabio, *Cement and Concrete Research*,
661 2015, **67**, 21–30.
- 662 66 J. Yoshikawa, J. A. Lewis and B.-W. Chun, *Journal of the American Ceramic Society*, 2009, **92**, S42–S49.
- 663 67 J. Gregory and S. Barany, *Advances in Colloid and Interface Science*, 2011, **169**, 1–12.
- 664 68 M. Kamibayashi, H. Ogura and Y. Otsubo, *Journal of Colloid and Interface Science*, 2008, **321**, 294–
665 301.
- 666



Synopsis: Coulombic repulsion alone is insufficient to mitigate aggregation of suspensions with strong charge screening behavior, whereas superior interparticle separations are created via steric hindrance when adsorbed layer thickness exceeds the Debye length.